

# Parametric Design and Analysis of Multiple-Beam Reflector Antennas for Satellite Communications

**Sudhakar K. Rao**

Boeing Satellite Systems, Inc., Antenna & Microwave Division  
M/S W-S12-V333, P.O. Box 92919, Los Angeles, CA 90009-2919 USA  
Tel: +1 (310) 662-7241; Fax: +1 (310) 416-5656; E-mail: sudhakar.k.rao@boeing.com

---

## Abstract

This paper presents the parametric design and analysis of multiple-beam reflector-antenna systems employed for satellite communications. It is based on extending the earlier work [1] by taking into account the efficiency of the horn and pointing error of the satellite in the design of the multiple-beam antennas (MBAs), and by analyzing the edge-of-coverage directivity and co-polar isolation (C/I) performance. Design and analysis equations are developed for the multiple-beam antennas using offset parabolic-reflector antennas by including various design parameters such as the number of reflectors, the number of frequency cells, the focal-length-to-diameter (F/D) ratio, the horn efficiency, and the pointing error. The analysis employs a quasi-Gaussian beam representation for the primary and secondary patterns in order to take into account the effect of the sidelobes. Results of the analysis given in this paper agree well with rigorous computations based on Physical Optics analysis of the antenna radiation. Design curves showing the impact of horn efficiency on the C/I performance of multiple-beam antennas are presented for various frequency-reuse schemes.

**Keywords:** Multibeam antennas; reflector antennas; aperture antennas; satellite communication; antenna radiation patterns; satellite antennas; multireflector antennas; offset reflector antennas

## 1. Introduction

Over the last few years, there has been a tremendous growth in the use of multiple-beam antenna (MBA) systems for satellite communications. Multiple-beam antennas are currently being used for direct-broadcast satellites (DBS), personal communication satellites (PCS), military communication satellites, and high-speed Internet applications. These antennas provide mostly contiguous coverage over a specified field of view on Earth by using high-gain multiple spot beams for downlink (satellite-to-ground) and uplink (ground-to-satellite) coverage. The design objectives for the multiple-beam antennas are (1) to maximize the minimum gain over the coverage region, and (2) to maximize the pattern roll-off outside the spot-beam area and to minimize the sidelobe radiation in order to maximize the frequency reuse. Multiple-beam antennas typically use either a single-aperture design with complex beamforming networks, or multiple-aperture designs without beamforming networks. They typically use three-cell, four-cell, or seven-cell frequency-reuse schemes in order to increase the effective bandwidth by several fold.

The design of single-aperture multiple-beam antennas has been described earlier [2, 3] by using the "basic-feed concept" and the "enhanced-feed concept." It was shown that the "enhanced-feed concept," using overlapping feed clusters, can achieve good electrical performance by using a complex beamformer that requires an element-sharing network and a beamforming network.

Dufort [4] and Ingerson et al. [5] also described design issues related to single-aperture multiple-beam antennas. Multiple-aperture multiple-beam antennas have the benefits of hardware simplicity and better electrical performance compared to single-aperture multiple-beam antennas, but at the expense of an increased number of apertures.

The analysis and design of multi-reflector multiple-beam antennas have been presented earlier [1, 6], using offset parabolic-reflector antennas with a single feed per beam. However, these multiple-beam antennas use conventional feed horns (dominant-mode conical horns and Potter horns). This paper extends the earlier analysis by taking into account the horn efficiency and the pointing error of the satellite. The horn-efficiency values can be increased up to 93% by generating multiple propagating modes within the horn, using step discontinuities. Simplified design equations as well as parametric curves are presented for the coverage gain and C/I (co-polar isolation) performance of the multiple-beam antenna as a function of the number of frequency cells and the horn efficiency. The analysis is based on using a modified Gaussian-beam representation for the primary and secondary patterns, such that the sidelobe levels are properly accounted for in the performance analysis of the multiple-beam antennas. It is shown that the results of the simplified analysis presented here agree well with rigorous computations based on the Physical Optics analysis of the reflector antennas.

## 2. Aperture and Beam Layout

The number of apertures and the beam layout of multiple-beam antennas depends on the satellite-system requirements, such as the frequency plan or the number of cells, the co-polar isolation requirements, beam size, spacecraft limitations for accommodating large reflectors, etc. A typical antenna configuration for Telesat's Anik-F2 satellite is shown in Figure 1. The hybrid payload consists of (a) a C-band shaped beam, covering Canada, CONUS (continental US), and Mexico, using an 85 in diameter dual-gridded shaped-reflector antenna; (b) a Ku-band shaped beam, covering Canada and CONUS, using an 85 in diameter dual-gridded shaped-reflector antenna; and (c) a Ka-band multiple-beam antenna, producing 45 contiguous spot beams covering Canada and CONUS. The multiple-beam antenna system consists of four 55 in diameter offset reflectors for downlink (20 GHz), four 36 in diameter offset reflectors for uplink (30 GHz), and two 20 in diameter reflectors for RF tracking. The multibeam antennas are located on the east

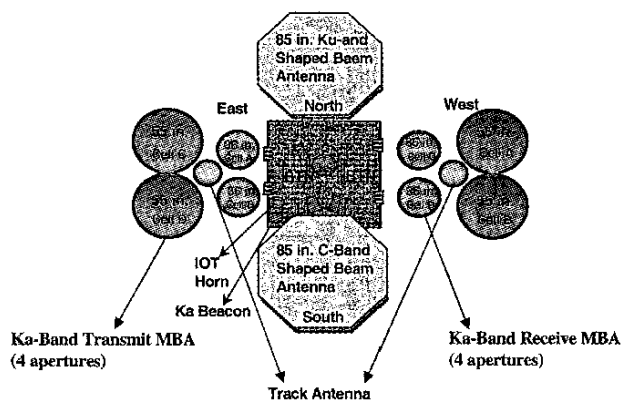


Figure 1. The antenna configuration of the Anik-F2 satellite, showing the Ka-band multiple-beam antennas (MBAs).

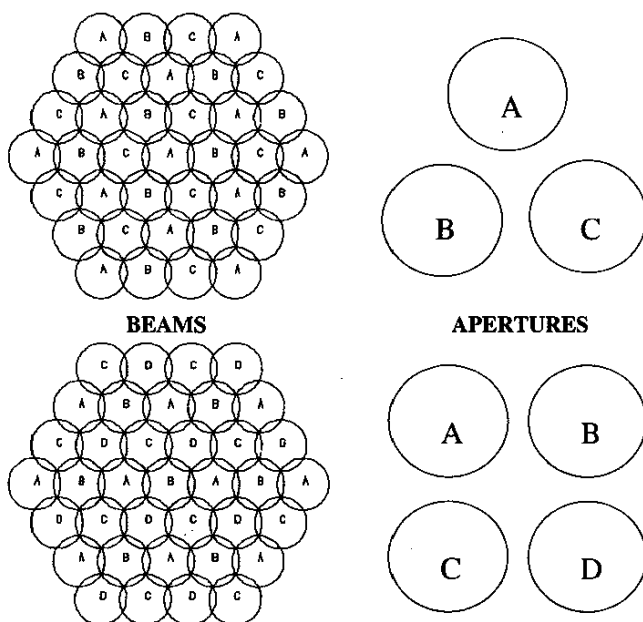


Figure 2. The beam-aperture layout of multiple-beam antennas using three and four apertures.

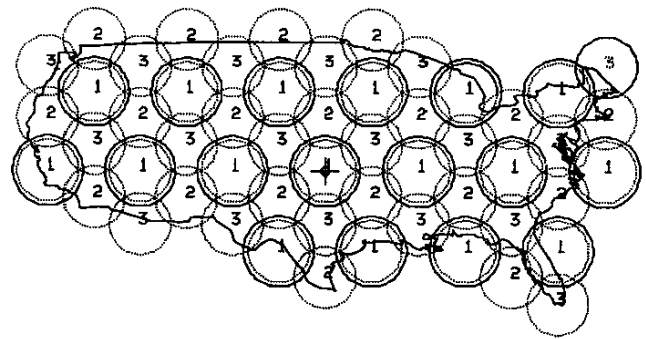


Figure 3a. CONUS (continental US) coverage with 54 spot beams using a three-cell frequency-reuse scheme (the solid circles are expanded by the pointing error).

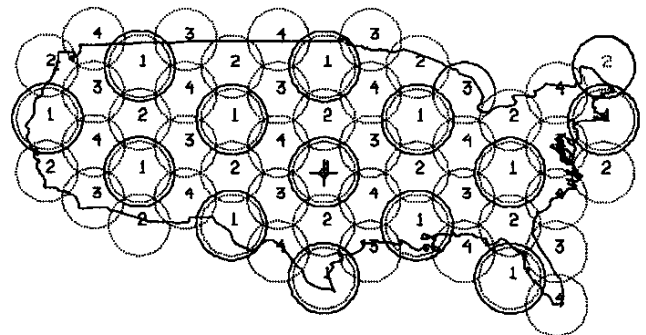


Figure 3b. CONUS coverage with 54 spot beams using a four-cell frequency-reuse scheme (the solid circles are expanded by the pointing error).

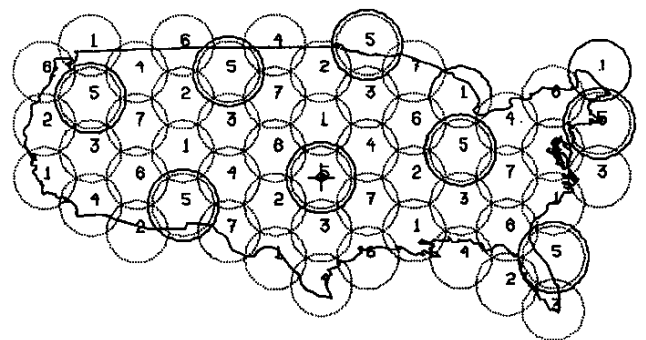


Figure 3c. CONUS coverage with 54 spot beams using a seven-cell frequency-reuse scheme (the solid circles are expanded by the pointing error).

and west sides of the spacecraft, as illustrated in Figure 1. Figure 2 shows the aperture and beam layouts using three- and four-aperture multiple-beam antennas. The number of apertures dictates the maximum size of the feed that can be used for the multiple-beam antennas. When compared to a single-aperture multiple-beam antenna, the feed size can be increased by a factor of 1.732 for a three-aperture design, by a factor of 2.0 for a four-aperture system, and by a factor of 2.646 for a seven-aperture system. Increased feed size for a multi-aperture system has the advantages of lower spillover loss and reduced sidelobe levels. A four-aperture multiple-beam antenna system is often proposed due to spacecraft pack-

aging and performance considerations, and is assumed here for the parametric design.

Figure 3 shows the beam layout using 54 spot beams covering CONUS with three-cell, four-cell, and seven-cell frequency-reuse schemes. The spacing between adjacent beams ( $\theta_s$ ) is  $0.606^\circ$ , and the beam size ( $\theta_0$ ) at the triple-beam crossover is  $0.7^\circ$ . The frequency-reuse factors are 18.00, 13.50, and 7.71 for the three-cell, four-cell, and seven-cell schemes, and are obtained by dividing the number of beams by the number of frequency cells. The closest spacings among beam centers reusing the frequency for the three-cell, four-cell, and seven-cell schemes are given respectively by [1, 2]

$$\theta^3 = 1.732\theta_s, \quad (1)$$

$$\theta_c^4 = 2.00\theta_s, \quad (2)$$

$$\theta_c^7 = 2.646\theta_s \quad (3)$$

The beam size needs to be expanded with the overall pointing error ( $\Delta\theta^P$ ) in order to evaluate the worst-case performance. The closest distance of the reuse beams from the beam peak is given by

$$\theta_L = \theta_c^N - 0.5\theta_0 - \Delta\theta^P. \quad (4)$$

Figure 4 shows the beam layout for a four-cell reuse scheme ( $N = 4$ ) and the various angles shown in the above equations.

### 3. Multiple-Beam Antenna Design

The design of the multiple-beam antenna starts with the beam-size requirement and the frequency plan. The beam size is defined as the diameter of the beam at the triple-beam crossover point, and is  $K$  dB below the beam peak (a typical value for  $K$  is about 4). The spacing between adjacent beams is 0.866 of the beam diameter. For a four-aperture multiple-beam antenna, the reflector size is obtained using the equation

$$\theta_0^K \cong 65 \left[ \frac{K}{3} \right]^{0.5} \frac{\lambda_L}{D}, \quad (5)$$

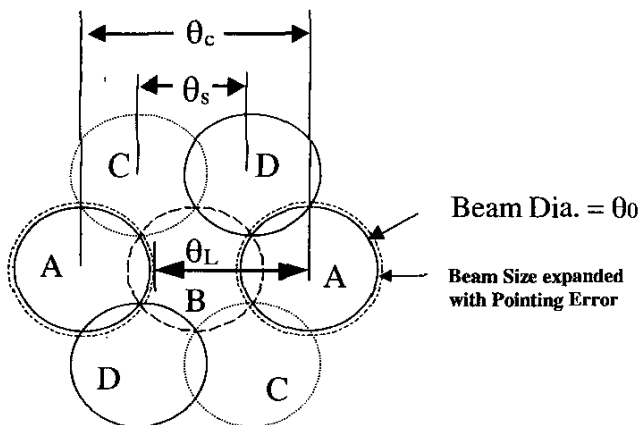


Figure 4. The angular parameters of a four-cell frequency-reuse multiple-beam antenna.

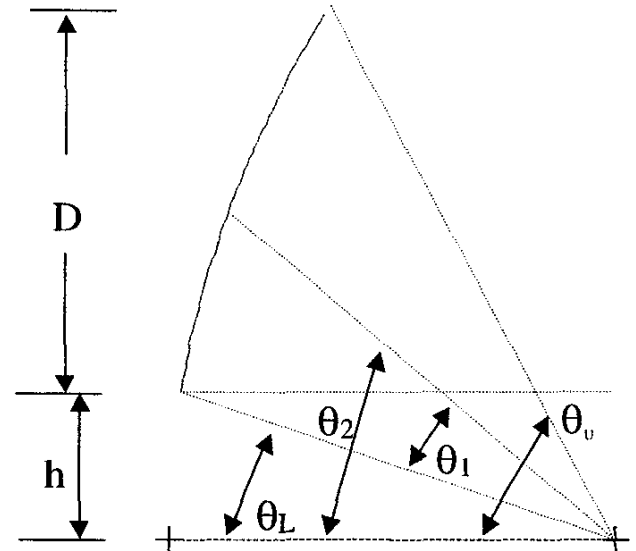


Figure 5. The offset parabolic-reflector geometry, showing the design parameters.

where  $\theta_0^K$  is the full beamwidth at  $K$  dB below the beam peak, and is approximately equal to  $(K/3)^{0.5}$  times the half-power beamwidth; and  $\lambda_L$  is the wavelength at the lowest frequency of the band. The constants relating the beamwidth to the normalized reflector size are 65.0, 75.0, and 83.9, for  $K = 3, 4,$  and  $5,$  respectively.

The  $F/D$  ratio of the reflector depends on the coverage region and the maximum number of beamwidths that need to be scanned, and is typically in the range 1.0 to 2.0. It also depends on the mechanical packaging issues on the spacecraft. For large scans (more than a four-beamwidth scan), a larger  $F/D$  is desired to minimize beam distortions caused by the coma lobes. The offset clearance,  $h$ , is selected such that the blockage-free condition is maintained for the maximum scanned beam, and is given approximately by

$$h \geq 2F \tan \theta_{sm}, \quad (6)$$

where  $\theta_{sm}$  is the maximum scan angle towards the reflector offset from the boresight direction. The above equation is often used by designers, but it does not take into account the feed-array size. The modified equation for the minimum angle without feed blockage that takes into account the feed-array size is given by

$$\theta_{SL} = \tan^{-1} \left[ \frac{h - (\theta_{sm} \cos \theta_2 / S_F)}{F - \frac{h^2}{4F} + (\theta_{sm} \sin \theta_2 / S_F)} \right] - \frac{1}{2} \tan^{-1} \left[ \frac{h}{F - \frac{h^2}{4F}} \right]. \quad (7)$$

The value of  $h$  needs to be selected such that  $\theta_{SL} > \theta_{sm}$ . The parameter  $\theta_2$  in the above equation is the reflector angle, shown in Figure 5, and  $S_F$  is the scan factor, which is explained later. The factor  $\theta_{sm}/S_F$  in Equation (7) can be replaced with the maximum dimension of the feed array from the focal point in the direction of the reflector offset.

The feed size is an important design parameter for the multiple-beam antenna design. It depends on the number of reflectors being used, and is independent of the frequency-reuse scheme. For a three-, four-, and seven-reflector multiple-beam antenna, the feed size,  $d_m$ , for a beam-spacing  $\theta_s$  is given by

$$d_m^{3,4,7} = K_1^{3,4,7} \theta_s / S_F. \quad (8)$$

$K_1$  is a constant, which is 1.732 for a three-aperture, 2.0 for a four-aperture, and 2.646 for a seven-aperture multiple-beam antenna. For the four-aperture multiple-beam antenna that was considered here, the value for  $K_1$  is 2.0.  $S_F$  in the above equation is the scan factor, which depends on the reflector geometry, and is given by [1]

$$S_F = \frac{1 + X \left(\frac{D}{4F}\right)^2}{1 + \left(\frac{D}{4F}\right)^2} \tan^{-1} \left[ \frac{1 + \cos \theta_2}{2F} \right], \quad (9)$$

where  $X = 0.30$  for  $T < 6$ , and  $X = 0.36$  for  $T \geq 6$ .  $T$  is the feed-illumination taper (positive dB) on the reflector edge. The angular parameters for the offset-reflector geometry shown in Figure 5 are given by

$$\theta_{1,2} = \frac{1}{2} \left[ \tan^{-1} \left\{ \frac{D+h}{F - \frac{(D+h)^2}{4F}} \right\} \mp \tan^{-1} \left\{ \frac{h}{F - \frac{h^2}{4F}} \right\} \right]. \quad (10)$$

#### 4. Feed Model

The feed radiation pattern is expressed initially as a Gaussian model to represent the main beam [1]:

$$E(\theta) = \exp \left[ -A(\theta/\theta_b)^2 \right], \quad (11)$$

where  $\theta_b$  is the half angle of the 3 dB beamwidth of the horn, and is expressed by

$$\theta_b = C_1 \frac{\lambda}{d_m}. \quad (12)$$

The constant  $C_1$  depends on the efficiency of the horn. In order to determine the constant values, three horn designs have been synthesized. They are the Potter horn, with an efficiency of about 74%; a medium-efficiency horn, with 83% efficiency; and a high-efficiency horn, with 93% efficiency. Figure 6 shows the normalized radiation patterns of the three horns in the  $\phi = 45^\circ$  plane. The Potter horn has low sidelobes and a broader pattern, while the high-efficiency horn has a narrow pattern and high sidelobe levels. Higher efficiency is achieved by generating the higher-order  $TE_{1m}$ -type modes using step junctions, which make the aperture illumination more uniform in both the E and H planes of the horn. It was found theoretically that for a uniform field distribution in the aperture plane of a circular horn, the  $TM_z$  modes must not be present in the aperture plane, and only the  $TE_{1m}$  modes are

desired. For a uniform amplitude distribution in the aperture plane, the ideal mode distribution is 1.0, 0.146, 0.071, etc., for the  $TE_{11}$ ,  $TE_{12}$ ,  $TE_{13}$ , etc., modes, respectively, and the corresponding phase distributions are  $0^\circ$ ,  $180^\circ$ ,  $0^\circ$ , etc., respectively. This particular distribution of modes not only makes the field distribution uniform, but also makes the transverse aperture fields aligned with the principal polarization. In reality, the mode distribution is slightly different than the ideal distribution, due to the fact that other higher modes are also generated, apart from the desired modes. Because of this, ideal 100% efficiency cannot be achieved for the high-efficiency multi-mode horns. For a given aperture size, the number of propagating  $TE_{1m}$  modes is finite. The step discontinuities essentially generate the desired propagating modes. The size of the step controls the amplitudes of the higher-order modes. The aperture size and the frequency of operation determine the location of the steps. For example, in the case of a four-wavelength-diameter horn, the location of the first step is where the diameter is about 1.7 wavelengths, in order to generate  $TE_{12}$  modes, and the location of the second step is where the diameter is about 2.7 wavelengths, to generate the  $TE_{13}$  mode.

The constant  $C_1$  is then obtained by using a quadratic interpolation of the above three horn designs, and is given by

$$C_1 = 31 - 0.0041(93 - \eta)^2 + 0.341(93 - \eta), \quad (13)$$

where  $\eta$  is the efficiency of the horn.

The above equation works well for efficiency values in the range of 70% to 95%. The feed-illumination taper on the reflector edge,  $T$ , is given by

$$T = -20 \log_{10} \left[ \exp \left\{ -0.3467 \left[ \theta_1 (d_m/\lambda) / C_1 \right]^2 \right\} \right]. \quad (14)$$

For a four-aperture system with  $\theta_1 = 20.95^\circ$ ,  $d_m = 1.78$  in, and  $\lambda = 0.592$  in, the on-axis directivity values were 18.19 dBi, 18.72 dBi, and 19.21 dBi, respectively, for the Potter, medium-efficiency, and high-efficiency horn designs. The edge-illumination taper values for  $\theta_1 = 20.95^\circ$  were 9.2 dB, 10.3 dB, and 12.4 dB for the Potter, medium-efficiency, and high-efficiency horns, respectively. The higher edge-illumination taper of the high-

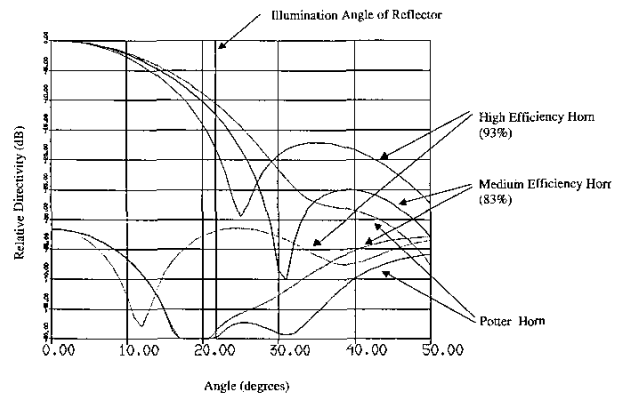


Figure 6. The radiation patterns of a 1.78 in circular horn in the  $45^\circ$  plane using Potter, medium-efficiency, and high-efficiency designs.

efficiency horn will broaden the main beam and lower the sidelobes of the multiple-beam antenna.

## 5. Secondary Pattern Analysis

The secondary patterns need to have an accurate model for performance analysis. They are represented by a quasi-Gaussian beam, where the main beam is represented as a Gaussian beam, the first sidelobe region is represented at a constant level, and the region beyond the first sidelobe is represented with a slope of  $-6$  dB per octave. The pattern shape is also a function of the horn-efficiency value. The secondary pattern in dB is given by [8]

$$G(\theta) = 10 \log_{10} \left\{ A \exp \left[ -B(0.866\theta/\theta_n)^2 \right] \right\}$$

in the region  $1.1547\theta_B \leq \theta \leq \theta_n$ , (15a)

$$= -30 \quad \text{in the region } \theta_n < \theta \leq 0.5(\theta_n + \theta_{s1}), \quad (15b)$$

$$= SL \quad \text{in the region } 0.5(\theta_n + \theta_{s1}) < \theta \leq \theta_{s1}, \quad (15c)$$

$$= SL - 20 \log_{10}(\theta/\theta_{s1}) \quad \text{in the region } \theta > \theta_{s1}. \quad (15d)$$

$G(\theta)$  is the gain in dB, and the constants in the above equation are given by

$$B = \frac{5.986}{\left( \frac{\theta_n}{1.1547\theta_B} \right)^2 - 1} \quad (16)$$

and

$$A = 0.398 \exp(B). \quad (17)$$

The 3 dB beamwidth of the reflector antenna is interpolated as follows:

$$\theta_3 = 2\theta_B = (0.058T^2 + 0.171T + 58.44)(\lambda/D). \quad (18)$$

The other parameters in the above equation are  $\theta_n$ , the position of first null;  $\theta_{s1}$ , the angular position of the first sidelobe; and  $SL$ , the sidelobe level relative to the beam peak (in dB). They are given by

$$\theta_n = (7.8 - 3.16SL)(\lambda/D), \quad (19)$$

$$\theta_{s1} = (30.25 - 3.07SL)(\lambda/D), \quad (20)$$

$$SL = -0.037T^2 - 0.376T - 17.6, \quad (21)$$

where  $D$  is the projected aperture of the reflector. The template model is compared to the computed pattern in Figure 7 for  $SL = -25$  dB. The analytical model agrees closely with the computed patterns in terms of half-power beamwidth and the location of the first null. The above equations are valid for feeds located close to the focal point of the reflector (or for beams close to the antenna's boresight). As the beams are scanned away from the antenna's boresight, the main impacts on antenna radiation are that the main beam broadens, the antenna gain deteriorates due to scan-

ning loss, and the sidelobe levels increase due to coma lobes. All three effects due to scanning are included in the analysis by modifying the above equations as follows [1, 4]:

$$\theta_3(\delta) = \theta_3 10^{0.05GL(\delta)}, \quad (22)$$

where  $GL(\delta)$  is the gain loss due to scan in dB, and is given by [1]

$$GL(\delta) = \frac{0.0015\delta^2}{\left[ (F/D_p)^2 + 0.02 \right]^2} + \frac{0.011\delta}{\left[ (F/D_p)^2 + 0.02 \right]}. \quad (23)$$

The increase in the sidelobe level due to scanning is obtained by quadratic interpolation:

$$SL(\delta) = SL(\delta=0) + \frac{0.36\delta}{\left[ (F/D_p)^2 + 0.02 \right]} - \frac{0.0026\delta^2}{\left[ (F/D_p)^2 + 0.02 \right]^2}. \quad (24)$$

$\delta$  in the above equations is the number of beamwidths scanned, and  $D_p$  is the diameter of the parent paraboloid ( $D_p = 2(D+h)$ ). The angular parameters shown in Equations (19) and (20) need to

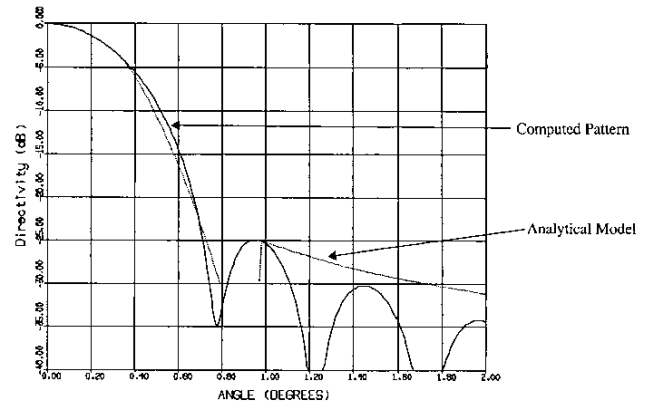


Figure 7. A comparison of the analytical model with the computed pattern for  $SL = -25$  dB.

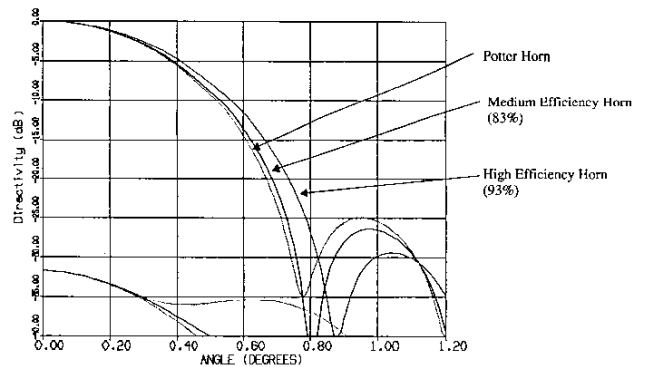


Figure 8. A comparison of the secondary patterns using the Potter, medium-efficiency, and high-efficiency horn designs shown in Figure 6.

be multiplied by the factor  $10^{0.05GL(\delta)}$  in order to account for the beam-broadening effect due to scanning.

Figure 8 compares the computed normalized radiation patterns of a 65 in diameter parabolic reflector using the three horn designs (Potter, medium-efficiency, and high-efficiency horns) shown in Figure 6. It can be seen that the high-efficiency horn gives broader patterns (lower edge-of-coverage gain) and lower sidelobe levels (improved co-polar isolation in most cases where interferers are in the sidelobe region).

## 6. Multiple-Beam Antenna-Performance Analysis

The electrical performance of the multiple-beam antenna, in terms of the beam directivity and co-polar isolation (C/I), can be analyzed using the following equations developed in this section. The minimum coverage area directivity, taking into account the pointing error ( $\Delta\theta^P$ ), is given by [1]

$$D_C = 10 \log_{10} \left[ \left( \frac{\pi D}{\lambda} \right)^2 \eta_i \right] - GL(\delta_m) - B(\delta_m) - 10 \log_{10} \left( \frac{0.5\theta_0 + \Delta\theta^P}{0.5\theta_0} \right)^2, \quad (25)$$

where  $\delta_m$  is the maximum number of beamwidths the antenna is scanned (defined as the ratio of maximum scan angle to the antenna half-power beamwidth at boresight direction). The first term in the above equation is the peak directivity for the boresight beam, the second term is the directivity loss due to scan for maximum scan angle, the third term is the peak-to-edge variation for the maximum scanned beam, and the last term is the directivity loss due to the pointing error. The antenna efficiency,  $\eta_i$ , is a function of the feed efficiency,  $\eta_f$ . A Potter horn has a lower taper on the reflector, but has very low spillover loss due to lower sidelobes. The high-efficiency horn, on the other hand, has higher taper on the reflector and high spillover loss (the sidelobe levels are around 19 dB below peak). The overall antenna efficiency,  $\eta_i$ , is a function of the illumination taper, the reflector geometry, and the feed efficiency, and is given by [7]

$$\eta_i = 4 \cot^2(\theta_1/2) \left[ 1 - \cos^n(\theta_1/2) \right]^2 \times \frac{n+1}{n^2} \left[ 1.025 + 0.5119(\eta_f - 0.74) - 7.542(\eta_f - 0.74)^2 \right]. \quad (26)$$

The above equation includes the aperture efficiency, the spillover efficiency, and the feed-horn efficiency. The value of the parameter  $n$  in the above equation is given by

$$n = \frac{-0.05T}{\log_{10} [\cos(\theta_1/2)]}. \quad (27)$$

An antenna efficiency value of about 82% is the maximum for a single reflector, and occurs for feed-taper values of about 10 dB [7]. Also, the efficiency value is better for smaller  $\theta_1$  values or lar-

ger  $F/D$  values. The parameter  $B(\delta_m)$  in Equation (25) is given by [1]

$$B(\delta_m) = 3 \left[ \frac{\theta_0}{\theta_3(\delta_m)} \right]^2. \quad (28)$$

The co-polar isolation (C/I) for the downlink antenna is usually more critical than for the uplink antenna, and is defined as the ratio of the co-polar directivity of the beam of interest to the combined directivity interference obtained by adding all the interferers, in power, over the beam of interest. It is to be noted that the cross-polar levels are not included in this analysis, due to the fact that the total interference is dominated by the co-polar signals from the adjacent beams re-using the same frequency. Self cross-polar interference can be almost neglected in most cases. The cell area of the beam needs to be expanded with the circular pointing error in order to compute the worst-case value (also, implementation margins necessary to account for the reflector-surface distortions and range uncertainties need to be added to all interferers to compute the co-polar isolation of spacecraft antennas, which are not included here). The combined interference signal due to  $J$  interferers onto the beam of interest is given by [1]

$$\sum_{j=1}^J I_j = 10 \log_{10} \left[ \sum_{j=1}^J \left( \frac{\pi D}{\lambda} \right)^2 \eta_{f_j} 10^{-0.1GL(\delta_j)} 10^{-0.1B_n \left( \frac{\theta_{js} + 0.5\theta_j - \Delta\theta^P}{0.5\theta_j} \right)^2} \right] \quad (29)$$

$\theta_j$  is the diameter of the  $j$ th interferer,  $\theta_{js}$  is the distance from the closest edge of the  $j$ th interferer to the beam of interest, and  $\Delta\theta^P$  is the maximum pointing error. The co-polar directivity,  $C$ , is equal to  $D_C$ , and is given by Equation (25). Based on Equations (25) and (29), the co-polar isolation, C/I, can be calculated. For example, the angles  $\theta_{js}$  of the closest six interferers for a four-cell scheme from Figure 4 are given by [1]

$$\theta_{1s} = \theta_{4s} = \theta_C - \theta_0, \quad (30)$$

$$\theta_{2s} = \theta_{6s} = \left[ \theta_C^2 + 0.25\theta_0^2 - 0.5\theta_C\theta_0 \right]^{0.5} - 0.5\theta_0, \quad (31)$$

$$\theta_{3s} = \theta_{5s} = \left[ \theta_C^2 + 0.25\theta_0^2 + 0.5\theta_C\theta_0 \right]^{0.5} - 0.5\theta_0. \quad (32)$$

## 7. Results

The analysis results are compared here using computations on a four-aperture 65 in diameter parabolic-reflector multiple-beam antenna, with a focal length of 74 in and an offset clearance of 24.5 in, at 19.95 GHz frequency. The feed size was 1.78 in diameter, and used the following three designs: (a) a Potter horn with 74% efficiency, (b) a medium-efficiency horn with 83% efficiency, and (c) a high-efficiency horn with 93% efficiency. For an un-scanned beam, the peak directivity values calculated using the above analysis were 49.95 dBi, 49.89 dBi, and 49.08 dBi for

the Potter, medium-efficiency, and high-efficiency horn designs, respectively, while the computations based on Physical Optics (PO) software gave 49.82 dBi, 49.79 dBi, and 48.92 dBi, respectively. The analytical values agreed to within 0.15 dB of the computations. The reduction in peak directivity for the high-efficiency horn relative to the Potter horn was due to a larger spillover loss, caused by high sidelobe levels. The half-power beamwidths calculated for the secondary patterns using Equations (18) and (14) were 0.60°, 0.615°, and 0.648° for the Potter, medium-efficiency, and high-efficiency horn designs, respectively, while the computed beamwidths using PO software were 0.604°, 0.61°, and 0.65°. The beam broadening due to higher efficiency was due to the larger illumination taper on the reflector caused by a narrower primary pattern. For a 107-wavelength reflector with an  $F/D$  of 1.324, a beam spacing of 0.472°, a feed diameter of 1.71 in (Potter horn), and using a four-cell reuse scheme, the calculated co-polar isolation value was 12.2 dB, and the computed value using the Physical Optics software was 12.5 dB.

The computed peak and edge-of-coverage (EOC) directivity values of a four-aperture multiple-beam antenna, with  $D = 65$  in,  $F = 74$  in,  $h = 24.5$  in,  $\lambda = 0.592$  in,  $d = 1.78$  in (feed aperture diameter),  $\theta_s = 0.606^\circ$ ,  $\theta_0 = 0.7^\circ$ , and  $\Delta\theta^P = 0.05^\circ$ , are shown in Figure 9. The multiple-beam antenna had 54 overlapping spot beams covering CONUS with four-cell frequency reuse (the coverage shown in Figure 2). The three curves shown in Figure 9 represent different horn designs: the Potter ( $\eta = 74\%$ ), medium-efficiency ( $\eta = 83\%$ ), and high-efficiency ( $\eta = 93\%$ ) horns. The

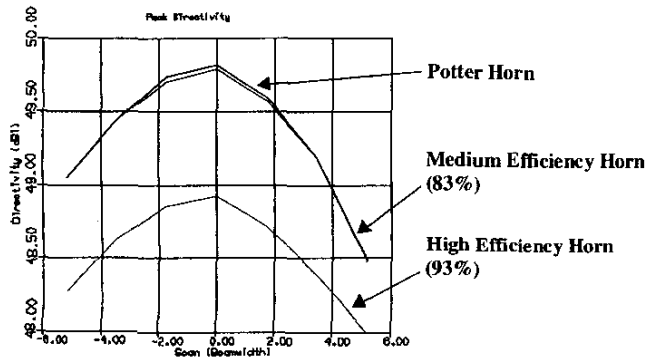


Figure 9a. The parametric variation of the peak directivity with scan and horn efficiency for a four-aperture multiple-beam antenna.

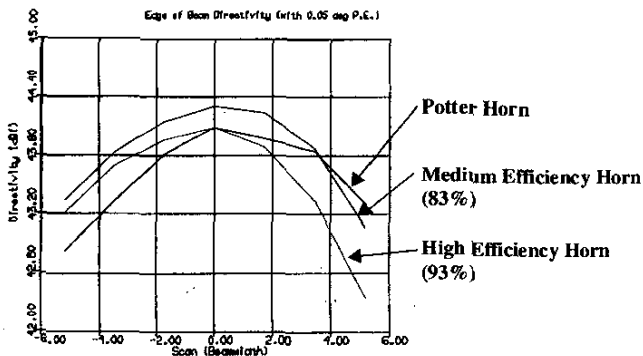


Figure 9b. The parametric variation of the edge-of-coverage directivity with scan and horn efficiency for a four-aperture multiple-beam antenna.

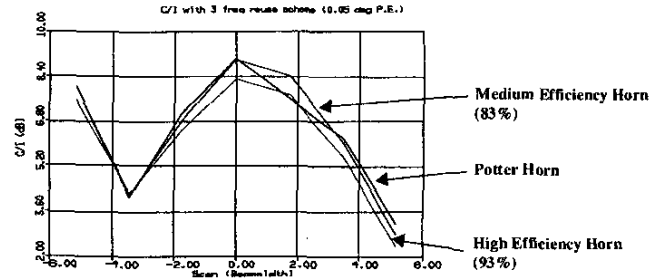


Figure 10a. The parametric variation of the aggregate co-polar isolation with scan and horn efficiency for a three-frequency re-use scheme for a four-aperture multiple-beam antenna.

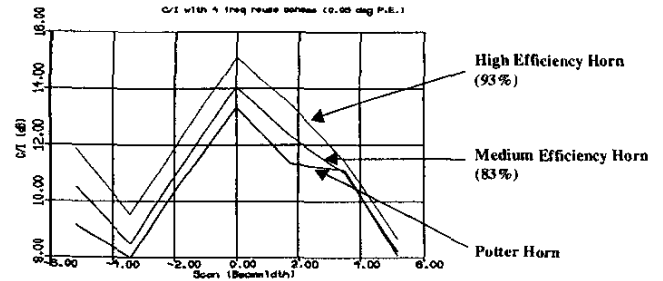


Figure 10b. The parametric variation of the aggregate co-polar isolation with scan and horn efficiency for a four-frequency re-use scheme for a four-aperture multiple-beam antenna.

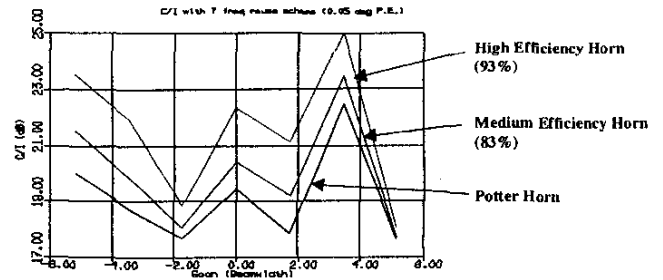


Figure 10c. The parametric variation of the aggregate co-polar isolation with scan and horn efficiency for a seven-frequency re-use scheme for a four-aperture multiple-beam antenna.

directivity variation with the number of beamwidths scanned is shown in Figure 9. The Potter and medium-efficiency horns were better in terms of coverage directivity. The use of a high-efficiency horn resulted in about 0.7 dB loss in edge-of-coverage directivity compared to a medium-efficiency horn, and about 0.9 dB loss, relative to a Potter horn. This was due to the following two reasons: (1) the high-efficiency horn caused increased spillover loss due to higher sidelobes of the primary patterns, and (2) the secondary beam broadened with the high-efficiency horn due to increased illumination taper on the reflector.

Figure 10 shows the computed co-polar isolation values of the multiple-beam antenna geometry shown above, using a four-aperture multiple-beam antenna (the parameters were the same as those used for Figure 9) with three-cell, four-cell, and seven-cell frequency-reuse schemes. The co-polar isolation values shown were the aggregate values (all co-polar interferers added in power),

and include a  $\pm 0.05^\circ$  pointing error. The non-monotonic behavior of the co-polar isolation performance with scan in Figure 10 was due to the beam-broadening effect causing the interfering signal shift from the sidelobe region to the main-beam roll-off region, and was also due to the appearance of the coma lobes. The co-polar isolation values for a three-cell reuse were better with a Potter horn. The use of a high-efficiency horn for the three-cell reuse deteriorated the co-polar isolation, due to main-beam broadening (note that the interferers were in the main-beam fall-off region rather than the sidelobe region for a three-cell scheme). A high-efficiency horn is not recommended for the three-cell reuse, due to inferior co-polar isolation and edge-of-coverage directivity performance; a Potter horn is optimum for such applications. For the four-cell and seven-cell reuse schemes, a high-efficiency horn gave about 1.5 dB and 2.5 dB (on average) co-polar isolation improvements, respectively, for beams scanned up to four beamwidths, compared to the Potter-horn design. The high-efficiency horn gave better overall performance for seven-cell reuse. For four-cell reuse, a high-efficiency or medium-efficiency horn needs to be used, depending on whether the interference is caused by the sidelobe or the main-beam region (which depends on the extent of the pointing error and beam rollover). The results shown in Figures 9 and 10 can be scaled to any  $F/D$  ratio of the reflector by using Equation (23), which relates  $F/D$  to the scan parameters.

## 8. Conclusions

The design and analysis of multiple-beam antennas using horn efficiency as a parameter have been detailed in this paper. It was shown that the overall multiple-beam antenna performance, in terms of edge-of-coverage directivity and co-polar isolation, could be modeled using primary-feed patterns. The following conclusions are drawn, based on the results shown here:

- Multiple-beam antenna performance can be optimized by the proper selection of the horn design.
- High-efficiency horns are better for a seven-cell reuse scheme, due to better overall performance. The co-polar isolation improves significantly, at the expense of the edge-of-coverage directivity.
- For a four-cell reuse scheme, either a high-efficiency or a medium-efficiency horn needs to be used for a four-aperture multiple-beam antenna, depending on sidelobe or main-beam interference.
- A Potter horn is optimum for the three-cell frequency-reuse scheme.
- For a three-aperture multiple-beam antenna, a high- or medium-efficiency horn gives better overall performance.

The design procedure described in this paper can be used for quick design and performance analysis of multiple-beam antennas.

## 9. Acknowledgements

The author would like to thank Dr. Chih-Chien Hsu, Mr. Jim Wang, and Dr. Arun Bhattacharyya for their contributions.

## 10. References

1. S. Rao, "Design and Analysis of Multiple-Beam Reflector Antenna," *IEEE Antennas and Propagation Magazine*, **41**, 4, August 1999, pp. 53-59.
2. S. Rao, "Development of a 45 GHz Multiple-Beam Antenna for Military Satellite Communications," *IEEE Transactions on Antennas and Propagation*, **AP-43**, 10, October 1995, pp. 1036-1047.
3. S. Rao, M. Cuchanski, and M. Tang, "Multiple Beam Antenna Concepts for Satellite Communications," ANTEM Symposium, Ottawa, Canada, 1984, pp. 289-292.
4. E. Dufort, "Optimum Low Sidelobe High Crossover Multiple Beam Antennas," *IEEE Transactions on Antennas and Propagation*, **AP-33**, Sept. 1985, p. 946.
5. P. Ingerson and C. A. Chen, "The Use of Non-Focusing Aperture for Multibeam Antenna," IEEE International Symposium on Antennas and Propagation *Digest*, 1983, pp. 330-333.
6. S. Rao, "Gaussian Beam Analysis of Multiple Beam Reflector Antennas," IEEE International Symposium on Antennas and Propagation *Digest*, Atlanta, 1998, pp. 2078-2081.
7. S. Rao and P. S. Kildal, "A Study of the Diffraction and Blockage Effects on the Efficiency of the Cassegrain Antenna" *Canadian Electrical Engineering Journal*, **9**, January 1984, pp. 10-15.
8. S. Rao and H. Moody, "Modeling of Shaped Beam Satellite Antenna Patterns," *IEEE Transactions on Antennas and Propagation*, **AP-35**, 6, June 1987, pp. 632-642.

## Introducing the Feature Article Author



**Sudhakar K. Rao** received the bachelor's degree in Electronics Engineering from the Regional Engineering College, Warangal, India, in 1974, the master's degree in Radar Systems Engineering from the Indian Institute of Technology, Kharaghpur, in 1976, and the PhD degree in Electrical Engineering from the Indian Institute of Technology, Madras, in 1980.

From 1976 to 1977, he worked as a Technical Officer at the Electronics Corporation of India Limited (ECIL), Hyderabad, and was involved with the design and test of LOS and TROPO communication antennas. He was a Research Assistant at the Indian Institute of Technology, Madras, during 1977-1980, and worked

on the application of GTD techniques for horn antennas. He worked as a Senior Scientific Officer at the Electronics and Radar Development Establishment (LRDE), Bangalore, from 1980 to 1981, and was involved with the design and analysis of phased-array radar antennas. From 1981 to 1982, he worked at the University of Trondheim, Norway, on Earth-station antennas, and had a post-doctoral fellowship from the Royal Norwegian Council for Scientific and Industrial Research (NTNF). He was a Research Associate at the University of Manitoba, Winnipeg, Canada, during 1982-1983, and worked on low-sidelobe antennas. From 1983-1996, he worked at Spar Aerospace Limited, Ste-Anne-de-Bellevue, Quebec, Canada, in Satellite Systems Design. There, he worked on commercial satellite payloads, mobile personal communication antennas, agile-beam antennas at EHF, and active antennas. He is currently working with Boeing Satellite Systems, El Segundo, California, as a Chief Scientist and Boeing Technical Fellow. He recently received Boeing's Special Invention Award for 2002 for his work on re-configurable satellites capable of operating in multiple orbital locations. His current interests are re-configurable antennas, multiple-beam antennas, and advanced payloads for both commercial and military applications.

Dr. Rao is a Senior Member of IEEE, and has published over 70 papers in technical journals and conferences in the area of microwave antennas and satellite communications. He has 12 US patents that have been awarded, and eight patents that are pending. His work on the modeling of satellite-antenna patterns was adopted by the CCIR in 1992. ☉



#### Editor's Comments *Continued from page 8*

have just heard reports of several people experiencing problems with *MathType* under *Word XP*, also known as *Word 2002* (a special "Thank you" to Chalmers Butler for bringing this to my attention). Furthermore, Design Science, the publishers of *MathType*, have produced a technical note (their TechNote 103, available at <http://www.mathtype.com/en/support/tsn/tsn103.htm>) on this problem. The consequences of the problem are serious enough that it is worth bringing it to our readers' attention, and explaining possible ways of mitigating those consequences.

The problem arises when you are working on a document in *Word XP* containing *MathType* equations, and something causes *Word XP* to shut down unexpectedly while the document is open (this could be caused by the operating system, or by another application, causing a "crash"). Upon restarting *Word XP*, *Word* "AutoRecovers" the document. However, some (or, unfortunately, in most cases, all) of the equations in the recovered document appear as pictures, instead of as OLE (object linking and embedding) objects that are editable in *MathType*. *MathType*'s TechNote 103 suggests a possible recovery process involving opening the document under a previous version of *Word* (e.g., *Word 2000* or *Word 97*). It is certainly worth trying the process described if you need to recover the equations in such a document. However, those of whom I'm aware who have tried this process have had relatively little – and in most cases, no – success with the procedure.

I suggest you take a couple of precautions that may allow you to recover most or all of work, should you experience such a problem. First, set *Word*'s automatic save function (Tools...Options...Save tab... "Save AutoRecovery info every \_\_\_ minutes" check box) to save the document very often: every minute might be appropriate on a desktop system. Second, uncheck the "Allow

fast saves" box. This forces *Word* to save the full document each time. Third, check the "Always create backup copy" box. This forces *Word* to save the currently saved copy of the document as filename.bak (where filename is the name of the document) before saving the current document to the AutoRecovery file. When you start *Word* after the unexpected shutdown and the AutoRecovery dialog box appears, you should then be able to open this prior version, instead of the possibly corrupted version in the AutoRecovery file (or you can choose not to have the document AutoRecovered, and open the .bak version of the document directly in *Word*). Another (or, even better, an additional) method of protecting yourself is to save a copy of the document – to a new file each time – quite often while working.

In my last column, I wrote about several "features" of *Word XP* that I found difficult to endure, at the least. Given the above problem, I am seriously considering going back to using *Word 2000* – or even *Word 97*!

### A Reminder Regarding the "Disk Full" Problem

Under *Word 97*, *Word 2000*, and *Word XP*, I and may others have experienced receiving one of several versions of messages saying that "the disk is full" when trying to save a *Word* document containing *MathType* equations (note that this may well happen with *Word* documents containing substantial numbers of other types of OLE objects, as well). This can happen whether saving the file is being done explicitly by the user, or by *Word* as part of its AutoRecovery function (in which case the message is often something to the effect that "AutoRecovery is being temporarily suspended"). This occurs in spite of the fact that there is really plenty of free space available on the hard drive. This has been a known issue with OLE objects and *Word* for many years. It is generally agreed that this occurs because some of the embedding information for one or more of the OLE objects in the document has become corrupted. In reading through the technical notes on the *MathType* support Web site, I realized that the method of recovering from this that had been recommended for a long time (and, indeed, that I have used with essentially 100% success for years) was no longer included in the recommended remedies. Although I covered this in a column years ago, I'm therefore repeating the information here.

When you receive a message of the above sort, cancel the "save" operation. Then, using File...Save As, choose "Rich Text Format (\*.RTF)" under "Save as Type." The document should be saved as an RTF file without a problem. In some cases, a warning to the effect that not all OLE objects could be saved may appear. Generally, you can ignore this. It is extremely rare that this has actually turned out to be true, in my experience. You then shut down *Word* completely (however, it is *not* necessary to reboot the computer). Re-start *Word*, open the RTF version of the document, and save it in .DOC format. The document should be undamaged, and subsequent saves should work fine – until the problem arises again, in which case repeating the procedure should again work.

After going through this process, you may very rarely observe one or two equations in which there has been some type of font substitution (this can often leave an equation looking as if it has been totally corrupted, particularly if a letter font has been substituted for a symbol or symbol-building font). In my experience, double-clicking on the equation to open it in *MathType*, making a

*Continued on page 49*